Nanoscience and Nanotechnology Letters
Vol. 11, 1–7, 2019

Omnidirectional THz Mirror on a One-Dimensional Porous Silicon Thermocrystal

B. Manzanares-Martínez[1] and J. Manzanares-Martinez[2,*]

[1] *Departamento de Fisica, Universidad de Sonora, Blvd. Luis Encinas y Rosales, Hermosillo, Sonora 83000, Mexico*
[2] *Departamento de Investigacion en Fisica, Universidad de Sonora, Blvd. Apartado Postal 5-088, Hermosillo, Sonora 83000, Mexico*

We have de designed a thermocrystal that reflects phononic thermal radiation. In the THz range, heat is kinetic energy carried predominantly by phononic vibrations. These mechanical vibrations have wavelengths that produces interferences within the internal interfaces of a phononic crystal. We determined conditions to obtain gaps simultaneously for longitudinal and transverse waves in a porous silicon multilayer. We propose a one-dimensional crystal with an omnidirectional mirror that reflects all phononic vibrations in the THz.

Keywords: Thermocrystal, Phononic Crystal, Omnidirectional.

1. INTRODUCTION

In a recent paper, Maldovan introduced the concept of thermocrystal, offering a new way to study thermal transmission [1]. Instead of using the traditional approach based on a flow of phonons as particles, this approach allows phonons to be treated as waves. The phonons vibrating in the THz range may experience interference with a crystal of nanometric period. This interference allows bandgaps for phonons, allowing new possibilities for controlling heat. The ability to manipulate thermal transport via interference-wave effects is of interest for technological applications [2].

In solids, heat is transported by vibrations and collision of molecules, free electrons, and phonons oscillating at a wide range of frequencies between $\nu = 0.1$ THz and $\nu =$ 100 THz. However, at the lowest limit of this range ($\nu <$ 0.1 THz), heat is mostly transported by phonons, which can be treated as waves, enabling undulatory control of heat flow [3].

The control of phonons as waves using phononic crystals (PnC) was proposed since 1993 [4]. In PnCs, the interference of mechanical waves allows for the existence of bandgaps, which lead to the creation of a vibrationless environment. Over time, bandgaps have been studied in the sonic (kHz) [5], ultrasonic (MHz) [6], and hypersonic regime (GHz) [7]. Unfortunately, as the frequency of the bandgap increases, the PnCs fabrication and characterization become more difficult [8]. To obtain bandgaps in the THz regime, we require a PnC with period of a few nanometers. At present, thermocrystals are only a theoretical idea and have not yet been fabricated in the laboratory. The first thermocrystal predicted to have gaps in the THz range was a two-dimensional crystal of $Si_{90}Ge_{10}$ [1]. This structure possesses a gap between 0.2 THz and 0.3 THz, considering a period of 10 nm.

A few years ago, Maldovan suggested that "*heat mirrors that provide all-angle wave reflection do not necessarily require three-dimensional period structures. One-dimensional multilayer system can be designed to achieve all-angle reflection for external thermal vibrations*" [3]. This proposal inspired us to carry out this work, in which we have found the conditions necessary to obtain a heat mirror with a one-dimensional lattice.

Heat mirrors may be of interest in various contexts, such as graphene-based devices [9–16]. Recently, thermal conductivity in suspended single-layer graphene has been studied, founding phenomena above the heat Fourier Law [17]. However, in practical applications, these graphene layers can not be placed over a heat-absorbing substratre, but require an ominidirectional mirror to avoid heat losses.

2. THEORY

Porous silicon lattices are formed by the periodic variation of layers of low and high mass density, ρ_l and ρ_h. The structure has a period of $d = d_l + d_h$, where d_l and d_h are the thickness of the low and high mass density, respectively. The layers with low mass densities allow

*Author to whom correspondence should be addressed.

the propagation of transverse and longitudinal waves with sounds speeds $c_{t,l}$ and $c_{l,l}$, respectively. In the same manner, the layers with high mass densities allow the propagation of transverse and longitudinal waves with sound speeds $c_{t,h}$ and $c_{l,h}$, respectively. The crystalline structure possesses periodicities of mass density, longitudinal sound speed, and transverse sound speed given by $\rho(z) = \rho(z+d)$, $c_l(z) = c_l(z+d)$, and $c_t(z) = c_t(z+d)$, respectively.

The phononic vibrations are described by the elastic wave equation,

$$-\omega^2\rho(z)u_i(\mathbf{x}) = \nabla\cdot\,[\rho(z)c_t^2(z)\nabla u_i(\mathbf{x})] + \nabla\cdot\left[\rho(z)c_t^2(z) \times \frac{\partial}{\partial x_i}\mathbf{u}(\mathbf{x})\right] + \frac{\partial}{\partial x_i}\{[\rho(z)c_l^2(z) - 2\rho(z)c_t^2(z)]\nabla\cdot\mathbf{u}(\mathbf{x})\} \quad (1)$$

Where the phononic-vector displacement is $\mathbf{u(x)}$ and the subscript i can be the coordinates x, y or z. Considering a propagation in the x–z plane, the waves have two polarizations. The first is the sagittal component, $\mathbf{u}_s(x,\ z) = [u_x(x,\ z),\ 0,\ u_z(x,\ z)]$; the second is the transverse component, $u_y(x,\ z)$. The wave equations for the x, y and z coordinates are

$$-\omega^2\rho(z)u_x(x,z) = \nabla_s\cdot\,[\rho(z)c_t^2(z)\nabla_s u_x(x,z)] + \nabla_s\cdot\left[\rho(z)c_t^2(z)\frac{\partial}{\partial x}\mathbf{u}_\mathbf{s}(x,z)\right] + \frac{\partial}{\partial x}\{[\rho(z)c_l^2(z) - 2\rho(z)c_t^2(z)] \times\nabla_s\cdot\mathbf{u}_\mathbf{s}(x,z)\} \quad (2)$$

$$-\omega^2\rho(z)u_z(x,z) = \nabla_s\cdot\,[\rho(z)c_t^2(z)\nabla_s u_z(x,z)] + \nabla_s\cdot\left[\rho(z)c_t^2(z)\frac{\partial}{\partial z}\mathbf{u}_\mathbf{s}(x,z)\right] + \frac{\partial}{\partial z}\{[\rho(z)c_l^2(z) - 2\rho(z)c_t^2(z)] \times\nabla_s\cdot\mathbf{u}_\mathbf{s}(x,z)\} \quad (3)$$

and

$$-\omega^2\rho(z)u_y(x,z) = \nabla_s\cdot\,[\rho(z)c_t^2(z)\nabla_s u_y(x,z)] \quad (4)$$

In these equations, we introduced the differential operator $\nabla_s = (\partial/\partial x, 0, \delta/\delta z)$.

2.1. Dispersion Relations

The plane wave method (PWM) is based in the Fourier series expansion [18]. The material parameters are described in series as

$$\rho(z) = \sum_{G_z}\rho(G_z)e^{iG_z z} \quad (5)$$

$$\rho(z)c_t^2(z) = \sum_{G_z}\tau(G_z)e^{iG_z z} \quad (6)$$

and

$$\rho(z)c_l^2(z) = \sum_{G_z}\Lambda(G_z)e^{iG_z z} \quad (7)$$

The calculation of the Fourier coefficients $\rho(G_z)$, $\tau(G_z)$, and $\Lambda(G_z)$ is presented in Appendix. To find the periodic waves, we consider the elastic-displacement vector as

$$\mathbf{u}(x,z) = e^{ik_x x}\sum_{G_z}\mathbf{u}(k_B, G_z)e^{i(k_B+G_z)z} \quad (8)$$

where the wave vector is $\mathbf{k} = (k_x, 0, k_B)$ and k_B is the periodic Bloch vector component in the z-direction. The reciprocal wave vectors are $G_z = (2\pi)/dn$, where n is an integer. To obtain an eigenvalue problem for the sagittal waves lying in the x–z plane, we substitute (5)–(8) into wave Eqs. (2) and (3), obtaining

$$\begin{bmatrix}\mathbf{M}_{xx} & \mathbf{M}_{xz}\\ \mathbf{M}_{zx} & \mathbf{M}_{zz}\end{bmatrix}\begin{bmatrix}\mathbf{u}_x\\ \mathbf{u}_z\end{bmatrix} = \omega^2\begin{bmatrix}\mathbf{N} & 0\\ 0 & \mathbf{N}\end{bmatrix}\begin{bmatrix}\mathbf{u}_x\\ \mathbf{u}_z\end{bmatrix} \quad (9)$$

The matrix elements $\mathbf{M}_{ij}$ and $\mathbf{N}$ are

$$M_{xx}(G_z, G_z') = k_x^2\Lambda(G_z - G_z') + (k_z + G_z)(k_z + G_z') \times \tau(G_z - G_z') \quad (10)$$

$$M_{xz}(G_z, G_z') = k_x(k_z + G_z')[\Lambda(G_z - G_z') - 2\tau(G_z - G_z')] + k_x(k_z + G_z)\tau(G_z - G_z') \quad (11)$$

$$M_{zx}(G_z, G_z') = k_x(k_z + G_z)[\Lambda(G_z - G_z') - 2\tau(G_z - G_z')] + k_x(k_z + G_z')\tau(G_z - G_z') \quad (12)$$

$$M_{zz}(G_z, G_z') = k_x^2\tau(G_z - G_z') + (k_z + G_z)(k_z + G_z') \times \Lambda(G_z - G_z') \quad (13)$$

and

$$N(G_z, G_z') = \rho(G_z - G_z') \quad (14)$$

In a similar manner, to obtain an eigenvalue problem for the transverse waves *uy*, we introduce (5), (6), and (8) into (4) to obtain

$$\mathbf{M}_{yy}\mathbf{u}_y = \omega^2\mathbf{N}\mathbf{u}_y \quad (15)$$

where

$$M_{yy}(G_z, G_z') = [k_x^2 + (k_z + G_z)(k_z + G_z')]\tau(G_z - G_z') \quad (16)$$

2.2. Phononic Reflection

To calculate the phononic reflection, we apply the boundary conditions at each interface of a multilayer crystal with N layers [18]. In this work, we consider isotropic solids. The elastic waves at a solid–solid interface have four boundary conditions. The first is the continuity of the normal displacement (u_z), the second is the tangential displacement (u_x and u_y), the third is the normal stress (σ_{zz}), and the fourth is the tangential stress (σ_{zx} and σ_{zy}).

For the third and fourth conditions, we need the stress tensor defined as

$$\sigma_{ik} = 2\rho c_t^2 u_{ik} + \rho(c_l^2 - 2c_t^2)u_{ll}\delta_{ik} \tag{17}$$

We start by considering the reflection of a phononic wave impinging from an incidence medium (ρ_i, $c_{l,i}$ and $c_{t,i}$) into the first layer (ρ_1, $c_{l,1}$ and $c_{t,1}$). Considering the continuity of normal displacement (u_z) at both sides of the first interface we have

$$\begin{aligned} &A_i \cos\propto_i + A_{tr}\sin\beta_i - A_{lr}\cos\propto_i \\ &\quad = \cos\propto_1 (M_l^{l+} - M_l^{l-}) + \sin\beta_1(-M_l^{t+} M_l^{t-}) \end{aligned} \tag{18}$$

where A_i is the amplitude of the incident longitudinal wave; A_{tr} and A_{lr} are the amplitudes of the reflected shear and longitudinal waves, respectively; and M_l^{l+} and M_l^{l-} are the first-layer longitudinal amplitudes moving forward and backward along the z-axis, respectively. In the same manner, M_l^{t+} and M_l^{t-} are the first-layer shear amplitudes moving forward and backward along the z-axis, respectively. The angle of the incident longitudinal wave is α_i. The angle of the transverse wave reflected is β_i. α_1 and β_1 are the angles for the longitudinal and transverse waves in the first layer. The angles are related by the Snell's law in the form

$$\frac{\sin\alpha_i}{c_{l,i}} = \frac{\sin\beta_i}{c_{t,i}} = \frac{\sin\alpha_1}{c_{l,1}} = \frac{\sin\beta_1}{c_{t,1}} \tag{19}$$

In the incident medium, $c_{l,i}$ and $c_{t,i}$ are the longitudinal and transverse sound velocities. $c_{l,1}$ and $c_{t,1}$ are those in the first medium. If we divide Eq. (18) by the amplitude A_i we obtain

$$\begin{aligned} &-\cos\propto_i a_{lr} + \sin\beta_i a_{tr} - \cos\propto_1 m_1^{l+} + \cos\propto_1 m_1^{l-} \\ &+\sin\beta_1 m_1^{t+} - \sin\beta_1 m_1^{t-} = -\cos\propto_i \end{aligned} \tag{20}$$

The boundary condition for the tangential amplitude (u_x) is

$$\begin{aligned} &\sin\propto_i a_{lr} + \cos\beta_i a_{tr} - \sin\propto_1 m_1^{l+} - \sin\propto_1 m_1^{l-} \\ &-\cos\beta_1 m_1^{t+} - \cos\beta_1 m_1^{t-} = -\sin\propto_i \end{aligned} \tag{21}$$

The continuity equation of the normal stress tensor (σ_{zz}) is

$$\begin{aligned} &\left(\rho_i c_{l,i} - 2\rho_i \frac{c_{t,i}^2}{c_{l,i}}\sin^2\alpha_i\right)a_{lr} - (\rho_i c_{t,i}\sin 2\beta_i)a_{tr} - \left(\rho_1 c_{l,1}\right. \\ &\left. - 2\rho_1 \frac{c_{t,1}^2}{c_{l,1}}\sin^2\alpha_1\right)m_1^{l+} - \left(\rho_1 c_{l,1} - 2\rho_1 \frac{c_{t,1}^2}{c_{l,1}}\sin^2\alpha_1\right)m_1^{l-} \\ &+(\rho_1 c_{t,1}\sin 2\beta_1)m_1^{t+} + (\rho_1 c_{t,1}\sin 2\beta_1)m_1^{t-} \\ &= -\left(\rho_i c_{l,i} - 2\rho_i \frac{c_{t,i}^2}{c_{l,i}}\sin^2\alpha_i\right) \end{aligned} \tag{22}$$

Finally, the continuity equation of the tangential stress tensor σ_{zx} is

$$\begin{aligned} &-\left(\rho_i \frac{c_{t,i}^2}{c_{l,i}}\sin 2\alpha_i\right)a_{lr} - (\rho_i c_{t,i}\cos 2\beta_i)a_{tr} \\ &\quad -\left(\rho_1 \frac{c_{t,1}^2}{c_{l,1}}\sin 2\alpha_1\right)m_1^{l+} + \left(\rho_1 \frac{c_{t,1}^2}{c_{l,1}}\sin 2\alpha_1\right)m_1^{l-} \\ &\quad -(\rho_1 c_{t,1}\cos 2\beta_1)m_1^{t+} + (\rho_1 c_{t,1}\cos 2\beta_1)m_1^{t-} \\ &\quad = -\left(\rho_i \frac{c_{t,i}^2}{c_{l,i}}\sin 2\alpha_i\right) \end{aligned} \tag{23}$$

For the internal interfaces, similar equations are obtained. In the final interface, only the forward components exist in the transmission medium. The boundary conditions for all the interfaces can be arranged in a matrix equation in the form

$$\mathbf{Ax} = \mathbf{b} \tag{24}$$

$\mathbf{A}$ is a $4(N+1)\times 4(N+1)$ matrix of the form

$$\mathbf{A} = \begin{bmatrix} \mathbf{M}_i & -\mathbf{M}_1 & 0 & \cdots & \cdots & \cdots & 0 & 0 & 0 \\ 0 & \mathbf{M}_1 & -\mathbf{M}_2 & \cdots & \cdots & \cdots & 0 & 0 & 0 \\ \vdots & \vdots & \ddots & \cdots & \cdots & \cdots & \iddots & \vdots & \vdots \\ 0 & 0 & \cdots & \mathbf{M}_{k-1} & -\mathbf{M}_k & 0 & \cdots & 0 & 0 \\ 0 & 0 & \cdots & 0 & \mathbf{M}_k & -\mathbf{M}_{k+1} & \cdots & 0 & 0 \\ \vdots & \vdots & \iddots & \cdots & \cdots & \cdots & \ddots & \vdots & \vdots \\ 0 & 0 & 0 & \cdots & \cdots & \cdots & \mathbf{M}_{N-1} & -\mathbf{M}_N & 0 \\ 0 & 0 & 0 & \cdots & \cdots & \cdots & 0 & \mathbf{M}_N & -\mathbf{M}_f \end{bmatrix} \tag{25}$$

The matrices $\mathbf{M}_i$, $\mathbf{M}_k$ and $\mathbf{M}_f$ are

$$\mathbf{M}_i = \begin{bmatrix} -\cos\propto_i & \sin\beta_i \\ \sin\propto_i & \cos\beta_i \\ \rho_i c_{l,i} - 2\rho_i \dfrac{c_{t,i}^2}{c_{l,i}}\sin^2\alpha_i & -\rho_i c_{t,i}\sin 2\beta_i \\ -\rho_i \dfrac{c_{t,i}^2}{c_{l,i}}\sin 2\alpha_i & \rho_i c_{t,i}\cos 2\beta_i \end{bmatrix} \tag{26}$$

$$\mathbf{M}_k = \begin{bmatrix} \cos\propto_k & -\cos\propto_k & -\sin\beta_k & \sin\beta_k \\ \sin\propto_k & \sin\propto_k & \cos\beta_k & \cos\beta_k \\ \rho_k c_{l,k} - 2\rho_k \dfrac{c_{t,k}^2}{c_{l,k}}\sin^2\alpha_k & \rho_k c_{l,k} - 2\rho_k \dfrac{c_{t,k}^2}{c_{l,k}}\sin^2\alpha_k & -\rho_k c_{t,k}\sin 2\beta_k & -\rho_k c_{t,k}\sin 2\beta_k \\ \rho_k \dfrac{c_{t,k}^2}{c_{l,k}}\sin 2\alpha_k & -\rho_k \dfrac{c_{t,k}^2}{c_{l,k}}\sin 2\alpha_k & \rho_k c_{t,k}\cos 2\beta_k & -\rho_k c_{t,k}\cos 2\beta_k \end{bmatrix} \tag{27}$$

and

$$\mathbf{M}_f = \begin{bmatrix} \cos\propto_f & -\sin\beta_f \\ \sin\propto_f & \cos\beta_f \\ \rho_k c_{l,k} - 2\rho_k \dfrac{c_{t,k}^2}{c_{l,k}} \sin^2\alpha_k & -\rho_k c_{t,k} \sin 2\beta_k \\ \rho_k \dfrac{c_{t,k}^2}{c_{l,k}} \sin 2\alpha_k & \rho_k c_{t,k} \cos 2\beta_k \end{bmatrix} \quad (28)$$

In the last matrix, ρ_f, $c_{l,f}$ and $c_{t,f}$ are the density, longitudinal velocity, and transverse velocity for the final medium. The array **x** contains all the normalized-amplitude waves in the form

$$x^T = \lfloor a_{lr}, a_{tr}, m_1^{l+}, m_1^{l-}, m_1^{t+}, m_1^{t-}, \ldots, m_N^{l+}, m_N^{l-}, m_N^{t+}, m_N^{t-}, a_{lf}, a_{tf} \rfloor \quad (29)$$

Finally, **b** is a vector with zero for all its components except for the following: $b_1 = -\cos\propto_i$, $b_2 = -\sin\propto_i$, $b_3 = -(\rho_i c_{l,i} - 2\rho_i c_{t,i}^2/c_{l,i}\sin^2\alpha_i)$, and $b_4 = -\rho_i c_{t,i}^2/c_{l,i}\sin 2\alpha_i$.

To obtain the reflected and transmitted energy, we need to know the elastic pointing vector for the incident longitudinal wave

$$\langle S_{l,i}\rangle = \frac{1}{2}\omega \mathbf{k}_{l,i}\rho_i c_{l,i}^2 |u_{l,i}|^2 \quad (30)$$

The reflected longitudinal and shear stress energies are

$$\langle S_{l,r}\rangle = \frac{1}{2}\omega \mathbf{k}_{l,r}\rho_i c_{l,i}^2 |u_{l,r}|^2 \quad (31)$$

and

$$\langle S_{t,r}\rangle = \frac{1}{2}\omega \mathbf{k}_{t,r}\rho_i c_{t,t}^2 |u_{t,r}|^2 \quad (32)$$

The longitudinal and shear reflectances are respectively

$$R_l = \frac{\langle S_{l,r}\rangle}{\langle S_{l,i}\rangle} = |u_{l,r}|^2 \quad (33)$$

and

$$R_t = \frac{\langle S_{t,r}\rangle}{\langle S_{l,i}\rangle} = \frac{c_{t,i}\cos\beta_i}{c_{l,i}\cos\alpha_i}|u_{l,r}|^2 \quad (34)$$

3. NUMERICAL RESULTS

In this work we analyze a porous silicon lattice formed by periodic alternation of two different porosities. We consider the following material parameters. First, the high and low mass densities are $\rho_h = 1,118.4$ kg/m^3 and $\rho_l = 955.3$ kg/m^3, respectively. Next, the longitudinal velocities are $c_{l,h} = 4,600$ m/s and $c_{l,l} = 4,300$ m/s. The transverse velocities are $c_{t,h} = 2,800$ m/s and $c_{t,l} = 2,100$ m/s. Finally, the period is $d = 37$ nm. All these parameters have been obtained experimentally in the laboratory [19].

We first consider waves that propagate parallel to the z-axis. For this particular case, the oscillations with transverse (*shear*) and longitudinal components are parallel and perpendicular to the surface layers, respectively. The allowed modes are obtained from Eq. (9). In Figure 1, we present a map of the bands as a function of the filling fraction $f = d_h/d$. The bands for the longitudinal and transverse polarizations have blue and red line patterns, respectively. The white regions are the coincidences of both bandgaps. The black line represents the filling fraction $f = 0.1$ and the green arrow shows a bandgap centered around $\nu = 0.236$ THz.

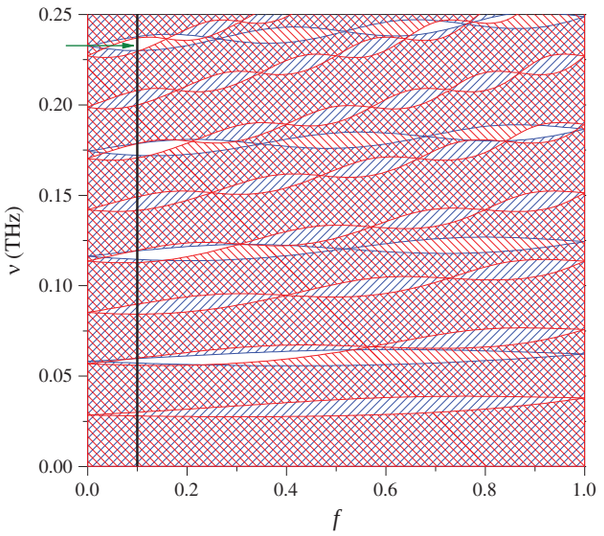

Fig. 1. Map of bands as function of the filling fraction f. The blue and red line-patterns represent the allowed bands for longitudinal and transverse polarization, respectively.

Considering the gap for $f = 0.1$ and $\nu = 0.236$ THz, we explore the propagation of waves with a wave vector parallel to the surface layers, k_x. An estimation of the mode polarization for $k_x > 0$ can be obtained by averaging the energy associated with each k_x component. In this manner, we can determine the longitudinal and transverse energy contributions for each vibration frequency. The details of the strain-energy-balance method were published by one of us in Ref. [18], where the **k**-dependence polarization of sagittal acoustic waves in phononic crystals was studied.

In Figure 2, we show the variation of the projected bands as a function of the wave vector parallel to the layers, k_x. At $k_x = 0$, the blue and red bands are purely longitudinal and transverse, respectively. We may also note that the bands with a small $k_x d$ component are predominantly longitudinal or transverse, for example, in the region with $k_x d < 1$. We observe that as we increase $k_x d$, the polarization changes, as at the limits of the white zone that represents the bandgap. The color scale illustrates longitudinal and transverse contributions in each band.

Now we turn our attention to propagation through a finite multilayer crystal considering diamond as the external medium. The longitudinal sound speed of diamond is $c_{l,d} = 17,500$ m/s. Even if the projected band structure in Figure 2 corresponds with an infinite crystal, it give us an

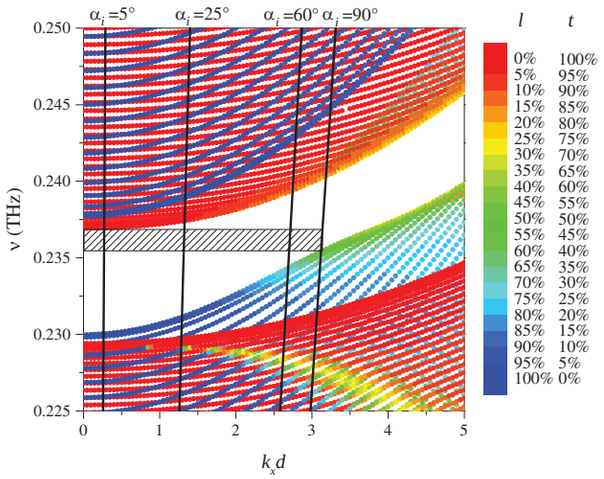

Fig. 2. Projected band structure of the sagittal polarization. The color maps correspond to longitudinal and shear modes. Black lines are the k_x components of a wave impinging from diamond with angles $\alpha_i = 5°$, 25°, 60° and 90°.

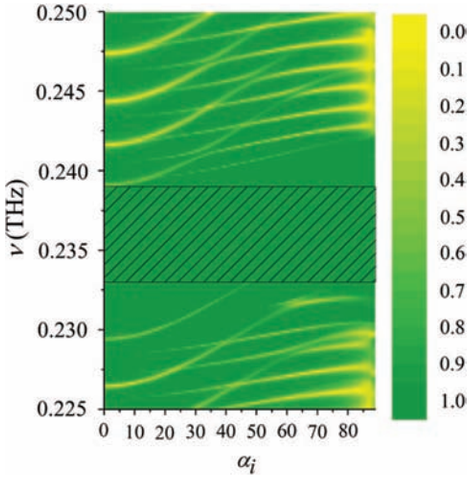

Fig. 4. Reflection of a heterostructure composed of three $(d_h d_l)^6$ porous silicon multilayers with periods of $d = 36.7$ nm, 37 nm, and 37.3 nm. An omnidirectional mirror exists for the black line-pattern area.

idea of propagation through a finite structure. The longitudinal wave obliquely incident on the sample has a wave vector parallel to the surface layers defined by the relation $k_x = (\omega/c_{l,d})\sin\alpha_i$. With black lines, we show the parallel wave vector corresponding to the incidence angle. From left to right, we have lines corresponding to the angles $\alpha_i = 5°, 25°, 60°$ and 90°. Depending on k_x, predominantly longitudinal, predominantly transverse, or mixed waves propagate over the multilayer. The black line-pattern area defines an omnidirectional mirror at which all phononic vibration impinging into the crystal will be reflected.

To verify the phononic omnidirectional mirror, we present the phononic reflection as a function of incidence angle (α_i) in Figure 3. In panels (a) and (b), we present the longitudinal and transverse reflectances R_l and R_t, respectively. The colormap illustrates the amount of energy reflected, where green and yellow represent complete and zero reflection, respectively. The multilayer is composed of 6 periods of low and high densities, plus and an additional layer of low density. In compact notation, the multilayer is defined as $(d_l d_h)^6 d_l$. In panel (c), we show the total energy reflected, that is the addition of longitudinal and transverse reflectances, $R_T = R_l + R_t$. We observe a complete stop band for all incidence angles in the black line-pattern area.

At this point, we derived the conditions necessary to have a phononic omnidirectional mirror in the THz range. However, the gap is too narrow. Does there exist some method to obtain a wider gap? We consider two simple strategies to do so. One possibility is to obtain a higher contrast between the two periodic materials; however this option frequently has strong experimental restrictions. The other method is to use heterostructures to enlarge the bandgap, as we did some years ago for PnC in the GHz range [20]. The idea is to add the bandgaps of several

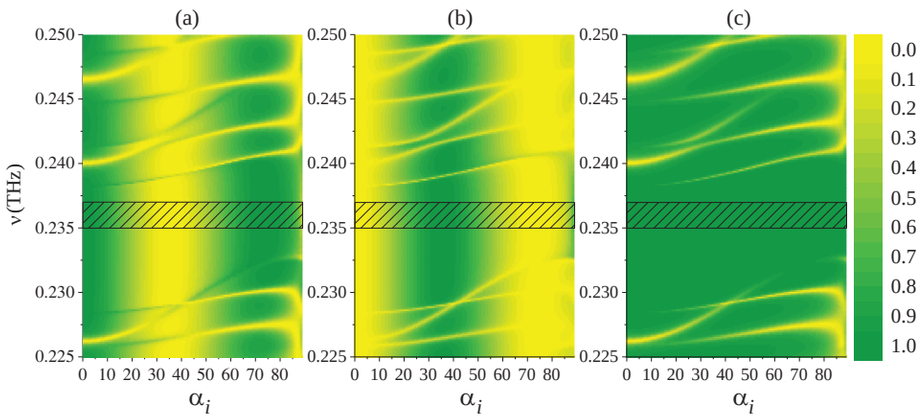

Fig. 3. Phononic reflection in the THz range. Panels (a and b) are the longitudinal and transverse reflected energies, R_l and R_t, respectively. Panel (c) is the total energy, R_T. The black line-pattern area is the omnidirectional mirror range.

multilayers crystals of different periods. As an example, we consider a porous silicon tandem structure of 3 multilayers of $(d_l d_h)^6$ with periods $d = 36.7$ nm, 37 nm, and 37.3 nm. In Figure 4, we observe that this heterostructure has an enlarged omnidirectional mirror from 0.233 THz to 0.239 THz.

4. CONCLUSIONS

We have determined the conditions necessary to have a one-dimensional porous silicon thermocrystal mirror in which phononic vibrations impinging from a diamond substrate are formally forbidden in the THz range. Considering that, at this frequency range, heat is mainly carried by phonons, this structure might reduce heat transport significantly. Even if the omnidirectional mirror range is narrow for porous silicon multilayers, it is still possible to enlarge it using heterostructures. We expect our results to illustrate the importance of phononic-wave interference for nanoscale thermal transport.

APPENDIX

The material parameters are described by the functions

$$\rho(z) = \rho_l + (\rho_h - \rho_l)\Theta\left(\frac{d_h}{2} - \lfloor z \rfloor\right) \tag{35}$$

$$\rho(z)c_t^2(z) = \rho_l c_{t,l}^2 + (\rho_{hc_{t,h}^2} - \rho_l c_{t,l}^2)\Theta\left(\frac{d_h}{2} - \lfloor z \rfloor\right) \tag{36}$$

and

$$\rho(z)c_l^2(z) = \rho_l c_{l,l}^2 + (\rho_{hc_{l,h}^2} - \rho_l c_{l,l}^2)\Theta\left(\frac{d_h}{2} - \lfloor z \rfloor\right) \tag{37}$$

where $\Theta(\xi)$ is the Heaviside function ($\Theta = 1$ if $\xi \geq 1$, and $\Theta = 0$ if $\xi < 0$). The Fourier coefficients are defined by the integrals

$$\rho(G_z) = \frac{1}{d}\int_{-d/2}^{d/2} \rho(z) e^{-iG_z z} dz \tag{38}$$

$$\tau(G_z) = \frac{1}{d}\int_{-d/2}^{d/2} \rho(z) c_t^2(z) e^{-iG_z z} dz \tag{39}$$

and

$$\Lambda(G_z) = \frac{1}{d}\int_{-d/2}^{d/2} \rho(z) c_l^2(z) e^{-iG_z z} dz \tag{40}$$

Calculating the integrals, we obtain

$$\rho(G_z) = [\rho_h + f(\rho_h - \rho_l)]\delta_{G_z,0} + \left\{\rho_h + \left[f(\rho_h - \rho_l) \times \frac{\sin(G_z d_h/2)}{G_z d_h/2}\right]\right\}(1 - \delta_{G_z,0}) \tag{41}$$

$$\rho(G_z) = [\rho_l c_{t,l}^2 + f(\rho_{hc_{t,h}^2} - \rho_l c_{t,l}^2)]\delta_{G_z,0} + \left\{\rho_l c_{t,l}^2 + \left[f(\rho_{hc_{t,h}^2} - \rho_l c_{t,l}^2)\frac{\sin(G_z d_h/2)}{G_z d_h/2}\right]\right\}(1 - \delta_{G_z,0}) \tag{42}$$

and

$$\Lambda(G_z) = [\rho_l c_{l,l}^2 + f(\rho_{hc_{l,h}^2} - \rho_l c_{l,l}^2)]\delta_{G_z,0} + \left\{\rho_l c_{l,l}^2 + \left[f(\rho_{hc_{l,h}^2} - \rho_l c_{l,l}^2)\frac{\sin(G_z d_h/2)}{G_z d_h/2}\right]\right\}(1 - \delta_{G_z,0}) \tag{43}$$

where $f = d_h/d$.

Acknowledgment: This work was supported by CONAYCT-Mexico under grant 373931.

References and Notes

1. Maldovan, M., **2013**. Narrow low-frequency spectrum and heat management by thermocrystals. *Physical Review Letters, 110*(2), p.025902.
2. Cahill, D.G., Braun, P.V., Chen, G., Clarke, D.R., Fan, S., Goodson, K.E., Keblinski, P., King, W.P., Mahan, G.D., Majumdar, A.M., Humphrey, J., Phillpot, S.R., Pop, E. and Shi, L., **2014**. Nanoscale thermal transport. II. 2003–2012. *Applied Physics Reviews, 1*(1), p.011305.
3. Maldovan, M., **2015**. Phonon wave interference and thermal bandgap materials. *Nature Materials, 14*(7), pp.667–674.
4. Kushwaha, M.S., Halevi, P., Dobrzynski, L. and Djafari-Rouhani, B., **1993**. Acoustic band structure of periodic elastic composites. *Physical Review Letters, 71*(13), p.2022.
5. Vasseur, J., Deymier, P.A., Khelif, A., Lambin, P., Djafari-Rouhani, B., Akjouj, A., Dobrzynski, L., Fettouhi, N. and Zemmouri, J., **2002**. Phononic crystal with low filling fraction and absolute acoustic band gap in the audible frequency range: A theoretical and experimental study. *Physical Review E, 65*(5), p.056608.
6. Manzanares-Martinez, B., Sanchez-Dehesa, J., Haakansson, A., Cervera, F. and Ramos-Mendieta, F., **2004**. Experimental evidence of omnidirectional elastic bandgap in finite one dimensional phononic systems. *Applied Physics Letters, 85*(1), pp.154–156.
7. Gorishnyy, T., Ullal, C.K., Maldovan, M., Fytas, G. and Thomas, E.L., **2005**. Hypersonic phononic crystals. *Physical Review Letters, 94*(11), p.115501.
8. Sledzinska, M., Graczykowski, B., Maire, J., Chavez-Angel, E., Sotomayor-Torres, C.M. and Alzina, F., **2019**. in *Advanced Functional Materials*, Wiley. p.1904434.
9. He, M.D., Wang, K.J., Wang, L., Li, J.B., Liu, J.Q., Huang, Z., Wang, L., Wang, L., Hu, W. and Chen, X., **2014**. Graphene-based terahertz tunable plasmonic directional coupler. *Applied Physics Letters, 105*(8), p.081903.
10. Xu, H., Li, H., He, Z., Chen, Z., Zheng, M. and Zhao, M., **2017**. Dual tunable plasmoninduced transparency based on silicon-air grating coupled graphene structure in terahertz metamaterial. *Optics Express, 25*(17), pp.20780–20790.
11. Cen, C., Chen, J., Liang, C., Huang, J., Chen, X., Tang, Yi, Z., Xu, X., Yi, Y. and Xiao, S., **2018**. Plasmonic absorption characteristics based on dumbbell-shaped graphene metamaterial arrays. *Physica E: Low-dimensional Systems and Nanostructures, 103*, pp.93–98.
12. Cen, C., Lin, H., Liang, C., Huang, J., Chen, X., Yi, Z., Tang, Y., Duan, T., Xu, X. and Xiao, X., **2018**. Tunable plasmonic resonance absorption characteries-tics in periodic H-shaped graphene arrays. *Superlattices and Microstructures, 120*, pp.427–435.
13. Huang, H., Xia, H., Guo, Z., Li, H. and Xie, D., **2018**. Polarization-insensitive and tunable plasmon induced transparency in a graphene-based terahertz metamaterial. *Optics Communications, 424*, pp.163–169.
14. Li, D., Huang, H., Xia, H., Zeng, J., Li, H. and Xie, D., **2018**. Temperature-dependent tunable terahertz metamaterial absorber for the application of light modulator. *Results in Physics, 11*, pp.659–664.

15. Xu, H., Xiong, C., Chen, Z., Zheng, M., Zhao, M., Zhang, B. and Li, H., **2018**. Dynamic plasmon-induced transparency modulator and excellent absorber-based terahertz planar graphene metamaterial. *Journal of the Optical Society of America B, 35*(6), pp.1463–1468.

16. Xu, H., Li, H., Chen, Z., Zheng, M., Zhao, M., Xiong, C. and Zhang, B., **2018**. Novel tunable terahertz graphene metamaterial with an ultrahigh group index over a broad bandwidth. *Applied Physics Express, 11*(4), p.042003.

17. Xu, X., Pereira, L.F., Wang, Y., Wu, J., Zhang, K., Zhao, X., Bae, S., Bui, C.T., Xie, R. and Thong, J., **2014**. Length-dependent thermal conductivity in suspended single-layer graphene. *Nature Communications, 5*(1), pp.1–6.

18. Manzanares-Martinez, B. and Ramos-Mendieta, F., **2007**. Sagittal acoustic waves in phononic crystals: *k*-dependent polarization. *Physical Review B, 76*(13), p.134303.

19. Parsons, L.C. and Andrews, G.T., **2009**. Observation of hypersonic phononic crystal effects in porous silicon superlattices. *Applied Physics Letters, 95*(24), p.241909.

20. Moctezuma-Enriquez, D., Rodriguez-Viveros, Y.J., Manzanares-Martinez, M.B., Castro-Garay, P., Urrutia-Banuelos, E. and Manzanares-Martinez, J., **2011**. Existence of a giant hypersonic elastic mirror in porous silicon superlattices. *Applied Physics Letters, 99*(17), p.171901.

Received: 11 November 2019. Accepted: 11 March 2020.